Orbital torque and efficient magnetization switching using ultrathin Co|Al light-metal interfaces: Experiments and modeling.

N. Sebe,[1] A. Pezo,[1] S. Krishnia,[1] S. Collin,[1]
J.-M. George,[1] A. Fert,[1] V. Cros,[1] and H. Jaffrès[1]

[1]*Laboratoire Albert Fert, CNRS, Thales,*
Université Paris-Saclay, 91767 Palaiseau, France

CONTENTS

I. MAGNETIZATION AT SATURATION

Ta(5) | Pt(8) | Co(t_{Co}) | Al(1.4) | Pt(3) multilayers	M_s (MA/m)	H_k^{eff} (T)
Co(0.55)	0.96	1.78
Co(0.7)	0.97	1.68
Co(0.9)	1.05	1.5
Co(1.2)	1.22	0.89
Co(1.4)	1.13	0.58
Ta(5) | Pt(8) | Co(t_{Co}) | Al(3) | Pt(3) multilayers		
Co(0.7)	1.14	1.72
Co(0.9)	1.18	1.7
Co(1.2)	1.19	1.0
Co(1.4)	1.14	0.70
Ta(5) | Pt(8) | Co(0.9) | Pt(3)	1.27	0.72
Ta(5) | Pt(8) | Co(0.9) | Pt_{Pt} | Al(3) | Pt(3) multilayers		
Pt(0.25)	1.04	1.35
Pt(0.5)	1.06	1.25
Pt(0.75)	1.12	1.05
Pt(1)	1.28	0.95
Pt(2)	1.39	0.78
Pt(3)	1.44	0.79

TABLE I. Saturation magnetization (Ms) measured via SQUID and perpendicular anisotropy field (K_s) acquired by AHE in our magnetic thin films (300 K).

II. AHE DATA - PHYSICAL PARAMETERS EXTRACTED FROM OUR CIP FITTING PROCEDURE.

The following table gathers the main physical parameters extracted from our fitting procedure applied to AHE data.

Parameters	Symbols	spin ↑	spin ↓
Co conductivity (S/m)	σ_{Co}	$\frac{\sigma_{Co}}{2(1-\beta_{Co})} = 7.4 \pm 1.0 \times 10^6$	$\frac{\sigma_{Co}}{2(1+\beta_{Co})} = 1.6 \pm 0.3 \times 10^6$
Pt conductivity (S/m)	σ_{Pt}	$2.5 \pm 0.5 \times 10^6$	$2.5 \pm 0.5 \times 10^6$
Al conductivity (S/m)	σ_{Al}	$7.0 \pm 2 \times 10^6$	$7.0 \pm 2 \times 10^6$
Co mean free path (nm)	λ_{Co}	7.0 ± 1	2.0 ± 0.3
Pt mean free path (nm)	λ_{Pt}	2.0 ± 0.5	2.0 ± 0.5
Al mean free path (nm)	λ_{Al}	6.0 ± 1.5	6.0 ± 1.5
Co Bulk asymmetry coefficient	β_{Co}	0.65 ± 0.05	
Co Spin Hall angle	θ_{Co}	0.02 ± 0.005	-0.02 ± 0.005
Pt Spin Hall angle	θ_{Pt}	0.22 ± 0.03	-0.22 ± 0.03
Pt|Co int. transmission	$T_{Pt/Co}$	$\frac{T_{Pt/Co}}{1-\gamma_{Pt/Co}} = 0.9 \pm 0.1$	$\frac{T_{Pt/Co}}{1+\gamma_{Pt/Co}} = 0.4 \pm 0.1$
Co|Al int. transmission	$T_{Co/Al}$	$\frac{T_{Co/Al}}{1-\gamma_{Co/Al}} = 0.1 \pm 0.05$	$\frac{T_{Co/Al}}{1+\gamma_{Co/Al}} = 0.1 \pm 0.05$
Al|Pt Interface transmission	$T_{Al/Pt}$	$T_{Al/Pt} = 0.2 \pm 0.1$	$T_{Al/Pt} = 0.2 \pm 0.1$
Pt|Co Interface asymmetry coefficient	$\gamma_{Pt/Co}$	0.4 ± 0.1	
Co|Al Interface asymmetry coefficient	$\gamma_{Co/Al}$	0	
Pt|Co specularity in reflection	$sp_{Pt/Co}$	0.2 ± 0.1	
Co|Al specularity in reflection	$sp_{Co/Al}$	0.15 ± 0.1	
Pt|Co spin-memory loss	$\delta_{Pt/Co}$	0.4 ± 0.1	
Co|Cu spin-memory loss	$\delta_{Co/Cu}$	0.25 ± 0.1	
Cu|Pt spin-memory loss	$\delta_{Cu/Pt}$	0.4 ± 0.1	
Co|Al spin-memory loss	$\delta_{Co/Al}$	negligible	

TABLE II. Physical parameters for bulk Pt, Co, Cu and Al and their interfaces extracted from our AHE fitting procedure. The conductivities σ are given in the unit of S.cm^{-1} and the electronic mean free path (λ) in the unit of nm.

III. TRANSVERSE SPIN-TRANSPORT MODEL FOR SOT INVOLVING SHE AND SPIN AND ORBITAL RASHBA INTERACTIONS.

In this appendix, we describe in details our model used for qualifying the transverse angular momentum accumulations and spin-currents in the multilayered structure originating from SHE and Rashba interfacial interactions. This model adapts the drift-precession-diffusion theory framework. This approach is complemented by introducing complex spin diffusion lengths accounting for spin precession in a ferromagnetic layer of finite thickness [1, 2]. This simplification for the treatment of the specific spin degree of freedom is possible in the limit of vanishing SOC (case of $3d$ ferromagnet). The same qualitative conclusion in favor of a generalized diffusion scheme for the transverse spin component is also deduced from the Keldysh formalism [3].

A. Complex decoherence length and SOT

We assume that in the Co ferromagnetic layer, besides the *transverse* momentum relaxation time τ_p, the spin-relaxation is described by: a longitudinal relaxation (spin-flip) time τ_{sf} (generally quite long), a transverse decoherence term (e.g. from magnon emission/absorption) τ_Δ (generally short), and a certain Larmor time τ_J due to precession. Noting $\tilde{\mu} = Tr\langle\Psi_{kn}|\hat{\sigma}|\Psi_{kn}\rangle$, the-out-of equilibrium spin density and J_σ the spin current, their coupled dynamics are given by [4] :

$$\frac{\partial\tilde{\mu}}{\partial t} = -\frac{\hat{\mu}}{\tau_\Delta} - \frac{\hat{\mu}}{\tau_{sf}} - \frac{\hat{\mu}\times\hat{e}_m}{\tau_J} - \frac{\partial\hat{J}_\sigma(z)}{\partial z} \tag{1}$$

$$\frac{\partial\hat{J}_\sigma}{\partial t} = -\frac{\hat{J}_\sigma}{\tau_\Delta} - \frac{\hat{J}_\sigma}{\tau_p} - \frac{\hat{J}_\sigma\times\hat{e}_m}{\tau_J} - \frac{\mathscr{D}_\perp}{\tau_p}\frac{\partial\hat{\mu}}{\partial z} \tag{2}$$

where $\hat{e}_m$ is the unit vector of the local magnetization $\hat{\mathbf{m}}$. For the following calculations, it is useful to note the reduced complex spin accumulation $\hat{\mu} = v_F(\hat{\mu}_x + i\hat{\mu}_y)$ and complex transverse spin-current $\hat{J}_\sigma = \hat{J}_{\sigma_x} + i\hat{J}_{\sigma_y}$. The correspondence between a characteristic time time τ_i and the characteristic length λ_i is:

$\lambda_i = v_F \tau_i$. In the steady state regime, $\frac{\partial}{\partial t} = 0$. We then define $\tilde{\lambda}_\mu = \left(\frac{1}{\lambda_\Delta} + \frac{1}{\lambda_{sf}} - \frac{i}{\lambda_J}\right)^{-1}$ and $\tilde{\lambda}_J = \left(\frac{1}{\lambda_\Delta} + \frac{1}{\lambda_p} - \frac{i}{\lambda_J}\right)^{-1}$ two complex scaling length. Noting $\mathscr{D}_\perp = \left(\frac{v_F^2 \tau_p}{3}\right)$ the diffusion constant, the combination of these two equations yields *in fine*:

$$\frac{\partial^2 \hat{\mu}}{\partial z^2} = \frac{\hat{\mu}}{\tilde{\lambda}_p^2} \quad \text{and} \quad \frac{\partial^2 \hat{J}_\sigma}{\partial z^2} = \frac{\hat{J}_\sigma}{\tilde{\lambda}_p^2} \tag{3}$$

where $\tilde{\lambda}_p$ is the common *propagation* scaling length. It is defined by $\tilde{\lambda}_p^2 = \tilde{\lambda}_\mu \tilde{\lambda}_J$. Its real part represents the decay of the transverse spin components (accumulation and current) in the ferromagnet while its imaginary part represents its precession feature.

1. *Generalized complex spin-resistance*

The characteristic lengths described above are specific to each layer. In order to accurately model diffusion between different layers, it is needed to include in the model the different electrical resistivity. This is dealt with by introducing a selective layer spin-resistance r^s. Generalizing the approach used to describe non-collinear spin transport, we define r^s as :

$$r^s = \left(\frac{1}{G_{sh}}\right) \sqrt{\frac{\tilde{\lambda_\mu}}{\tilde{\lambda_J}}} \tag{4}$$

Regarding non magnetic materials, where λ_Δ and λ_J are zero, this writes: $(G_{sh} r^s) = \sqrt{\frac{\tau_{sf}}{\tau_p}}$. For instance, in Pt, $(G_{sh} r^s) \simeq 2$ as obtained from THz emission experiment [5]. It is greater than 1 as in all materials where $\tau_{sf} > \tau_p$. Notably, in low SOC materials as Cu or Al, it is typically larger than 10. In non collinear ferromagnets, the spin-resistance is complex, rendering spin precession.

2. *Relation between SOT and spin currents*

Spin-orbit torques $\hat{\Gamma}_{SOT}$ are defined as the time variations of the magnetization vector $\hat{\mathbf{m}}$ when an out-of-equilibrium spin current occurs which is opposite to the torque generated on the spin-accumulation $\hat{\mu}$ (in the limit of small SOC). From

total angular momentum conservation, the sign of the cross product term has then to be opposite to that of Eqn. [1]:

$$\hat{\Gamma}_{SOT} = \int_{\mathscr{V}} \frac{\partial \hat{\mathbf{m}}}{\partial t} d\mathscr{V} = -\int_{\mathscr{V}} \frac{\hat{e}_m \times \hat{\mu}}{\tau_J} d\mathscr{V} \tag{5}$$

From Eqn. [1], we have:

$$\hat{\mu} = -\tau_J \left(\frac{i + \tau_J \left(\frac{1}{\tau_\Delta} + \frac{1}{\tau_{sf}} \right)}{1 + \left[\tau_J \left(\frac{1}{\tau_\Delta} + \frac{1}{\tau_{sf}} \right) \right]^2} \right) \frac{\partial \hat{J}_\sigma}{\partial z}$$

and $\hat{\mu} \times \hat{e}_m = -i\hat{\mu}$ leading to:

$$\int_{\mathscr{V}} \frac{\hat{\mu} \times \hat{e}_m}{\tau_J} d\mathscr{V} = -\int_{\mathscr{V}} \frac{1 + i\tau_J \left(\frac{1}{\tau_\Delta} + \frac{1}{\tau_{sf}} \right)}{1 + \left[\tau_J \left(\frac{1}{\tau_\Delta} + \frac{1}{\tau_{sf}} \right) \right]^2} \left(\frac{\partial \hat{J}_\sigma}{\partial z} \right) dz$$

The integral over the volume of $\frac{\partial J_\sigma}{\partial z}$ yields the integrated torque Γ_{SOT} in the FM thickness we are searching for:

$$\hat{\Gamma}_{SOT} = \left(\frac{1 + i\tau_J \left(\frac{1}{\tau_\Delta} + \frac{1}{\tau_{sf}} \right)}{1 + \left[\tau_J \left(\frac{1}{\tau_\Delta} + \frac{1}{\tau_{sf}} \right) \right]^2} \right) \left(\hat{J}_\sigma^{in} - \hat{J}_\sigma^{out} \right) \tag{6}$$

This equation teaches us that the torques applied on the ferromagnetic layer are proportional to the balance between spin current *entering* through one interface $\hat{J}_\sigma^{in}$ and outgoing through the other interface $\hat{J}_\sigma^{out}$. The proportionality constant is complex, accounting for precession of the spin current around the magnetization. The real part of the resulting $\hat{\Gamma}_{SOT}$ is the damping like torque component while the imaginary part is the field like torque. In the following, we will propagate the spin currents between the different layers of our samples. From the latter equation, we can observe that the ratio between the Field-like and the Damping-like torques are closely dependent on the ratio between τ_J and τ_Δ. For thick FM layers, thicker than the decoherence length, an increase of the decoherence rate τ_Δ^{-1} enhances the Field-like term (from almost zero) and reduces the Damping-like component.

B. Multiple scattering approach (case of ultrathin layers)

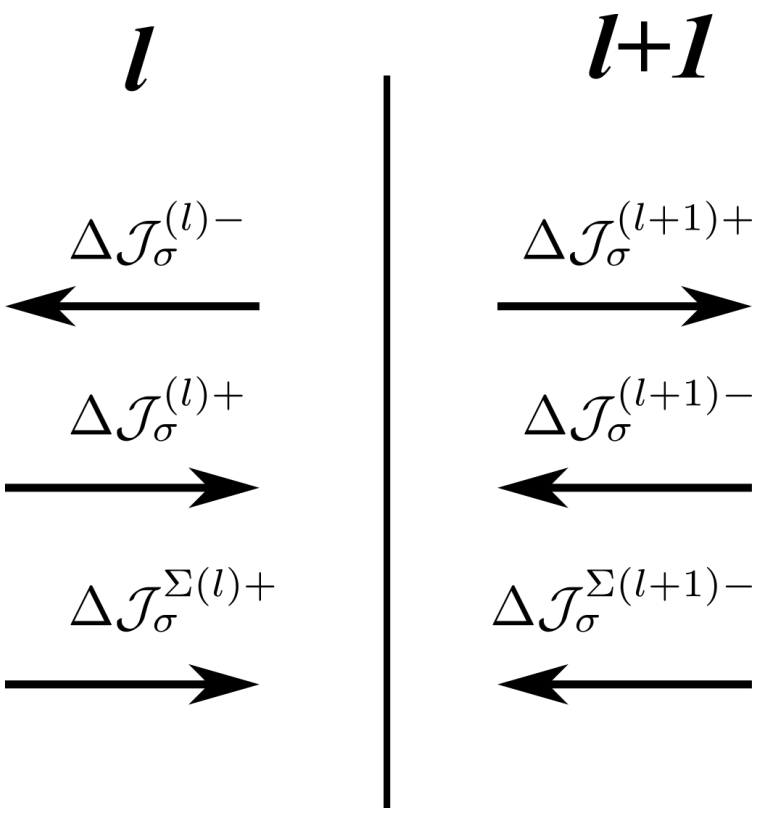

FIG. 1. Definition of the different spin currents terms, either incoming spin-current source $\Delta\hat{J}_\sigma^\Sigma$ or out-going out-of-equilibrium spin-current $\Delta\hat{J}_\sigma$ at one single interface

From now on, we note the spin-polarized current by $\Delta\hat{J}_\sigma = \left(J_\uparrow - J_\downarrow\right)$.

Estimating the spin currents $\hat{J}_\sigma^{in}$ and $\hat{J}_\sigma^{out}$ in the ferromagnetic layer of Pt | Co | Al | Pt is challenging due to the presence of different spin current sources and multiple interfaces scattering. We have to consider multiple scattering processes at several interfaces and boundaries. Our approach consists in a multiple-scattering formalism that enables to write a super-scattering matrix $\mathbb{S}$ from each individual interface scattering matrix $\tilde{S}$.

Let's consider a single interface between layers l and $l+1$ (figure 1). The purpose of a scattering matrix is to write a linear relationship between the two *outgoing* spin-accumulation flow (spin-currents) to the left and to the right, respectively $\Delta\hat{J}_\sigma^{(l)-}$ and $\Delta\hat{J}_\sigma^{(l+1)+}$, connected to the two *ingoing* spin-current $\Delta\hat{J}_\sigma^{(l)+}$ and $\Delta\hat{J}_\sigma^{(l+1)-}$. This also may involve two sources terms (SHE) generated from either

side materials $\Delta\hat{J}_\sigma^{\Sigma(l)+}$ and $\Delta\hat{J}_\sigma^{\Sigma(l+1)-}$. Because the source term imposes different boundary conditions, we need to consider two different scattering matrices, respectively S and $\tilde{S}$:

$$\begin{vmatrix} \Delta\hat{J}_\sigma^{(l)-} \\ \Delta\hat{J}_\sigma^{(l+1)+} \end{vmatrix} = \tilde{S} \begin{vmatrix} \Delta\hat{J}_\sigma^{(l)+} \\ \Delta\hat{J}_\sigma^{(l+1)-} \end{vmatrix} + S \begin{vmatrix} \Delta\hat{J}_\sigma^{\Sigma(l)+} \\ \Delta\hat{J}_\sigma^{\Sigma(l+1)-} \end{vmatrix}$$

or equivalently:

$$\begin{vmatrix} \Delta\hat{J}_\sigma^{(l)-} \\ \Delta\hat{J}_\sigma^{(l+1)+} \end{vmatrix} = \tilde{S} \left[\begin{vmatrix} \Delta\hat{J}_\sigma^{(l)+} \\ \Delta\hat{J}_\sigma^{(l+1)-} \end{vmatrix} + \tilde{S}^{-1} S \begin{vmatrix} \Delta\hat{J}_\sigma^{\Sigma(l)+} \\ \Delta\hat{J}_\sigma^{\Sigma(l+1)-} \end{vmatrix} \right]$$

thus defining $\tilde{S}^{-1} S \begin{vmatrix} \Delta\hat{J}_\sigma^{\Sigma(l)+} \\ \Delta\hat{J}_\sigma^{\Sigma(l+1)-} \end{vmatrix}$ as the *effective spin-current source* terms. Such formulation is able to treat the multiple diffusion character of the spin-transport within the multilayer.

1. *Single interface scattering matrix*

It turns out that each single scattering matrix at a given interface between two semi-infinite materials is written as:

$$\tilde{S}_l = \begin{bmatrix} \tilde{R}_l & \tilde{T}_l' \\ \tilde{T}_l & \tilde{R}_l' \end{bmatrix} \quad \text{and} \quad S_l = \begin{bmatrix} R_l & T_l' \\ T_l & R_l' \end{bmatrix} \tag{7}$$

where $\tilde{R}_l$ (resp. R_l) is the reflection coefficient for a spin-current (resp. for a source term) arriving from layer l to the interface between l and $l+1$; whereas $\tilde{T}_l$ (resp. T_l) is the corresponding transmission coefficient for a spin current (resp. for a source term) arriving from layer l to the interface between l and $l+1$. The coefficients noted with $'$ are the equivalent coefficients for the opposite flow direction on the same interface. We have derived those coefficients from the boundary conditions that we impose on the interface. The general self-consistent solutions can then be solved by using either $\Delta\hat{J}_\sigma^{(l)\pm}$ or $\Delta\hat{\mu}_\sigma^{(l)\pm}$ as relevant physical quantities. We chose the $\Delta\hat{J}_\sigma^{(l)\pm}$ basis able to treat both SHE and REE. Those are:

(i) the continuity of the total current when the spin-memory loss is zero giving:

$$\hat{J}_{\sigma}^{\Sigma(l)+} - \Delta\hat{J}_{\sigma}^{(l)-} + \Delta\hat{J}_{\sigma}^{(l)+} = -\hat{J}_{\sigma}^{\Sigma(l+1)+} + \Delta\hat{J}_{\sigma}^{(l+1)+} - \Delta\hat{J}_{\sigma}^{(l+1)-} \tag{8}$$

(ii) equality between diffusive spin-current and interfacial spin-current parameterized by the spin-mixing conductance ($G_{\uparrow\downarrow} = T\ G_{Sh}$) according to:

$$\begin{aligned} &\hat{J}_{\sigma}^{\Sigma(l)+} - \Delta\hat{J}_{\sigma}^{(l)-} + \Delta\hat{J}_{\sigma}^{(l)+} = \\ &= G_{\uparrow\downarrow}\left[r^{s(l)}\left(\Delta\hat{J}_{\sigma}^{(l)-} + \Delta\hat{J}_{\sigma}^{(l)+}\right) - r^{s(l+1)}\left(\Delta\hat{J}_{\sigma}^{(l+1)-} + \Delta\hat{J}_{\sigma}^{(l+1)+}\right)\right] \end{aligned} \tag{9}$$

when the spin-memory loss is absent.

(iii) When necessary, the introduction of a fictitious layer interface of evanescent thickness t_{loss} with spin-diffusion length λ_{loss} taking into account the previously defined spin-memory loss parameter δ owing to $\delta = \left(\frac{t_{loss}}{\lambda_{loss}}\right)$. This yields the formulae of $\tilde{R}_l$ and $\tilde{T}_l$ as a function of material and interface parameters according to:

$$\tilde{T}_l = \frac{2\ T_{\uparrow\downarrow}\ \tilde{r}_s^{(l)}\left(\frac{\delta}{\sinh\delta}\right)}{1 + \delta\coth(\delta)T_{\uparrow\downarrow}\left(\tilde{r}_s^{(l)} + \tilde{r}_s^{(l+1)}\right) + \delta^2 T_{\uparrow\downarrow}^2\tilde{r}_s^{(l)}\tilde{r}_s^{(l+1)}} \tag{10}$$

$$\tilde{R}_l = \frac{1 + \delta\coth(\delta)\ T_{\uparrow\downarrow}\left(\tilde{r}_s^{(l+1)} - \tilde{r}_s^{(l)}\right)}{1 + \delta\coth(\delta)T_{\uparrow\downarrow}\left(\tilde{r}_s^{(l)} + \tilde{r}_s^{(l+1)}\right) + \delta^2 T_{\uparrow\downarrow}^2\tilde{r}_s^{(l+1)}\tilde{r}_s^{(l+1)}} \tag{11}$$

Regarding S matrices dealing with the scattering of the source terms, the current discontinuity equation remains unchanged. However, contrary to the previous case, the source term does not solely derive from a spin accumulation. R_l and T_l then become:

$$T_l = \frac{T_{\uparrow\downarrow}\ \tilde{r}_s^{(l)}\left(\frac{\delta}{\sinh\delta}\right)}{1 + \delta\coth(\delta)T_{\uparrow\downarrow}\left(\tilde{r}_s^{(l)} + \tilde{r}_s^{(l+1)}\right) + \delta^2 T_{\uparrow\downarrow}^2\tilde{r}_s^{(l)}\tilde{r}_s^{(l+1)}} \tag{12}$$

$$R_l = \frac{1 + \delta\coth(\delta)\ T_{\uparrow\downarrow}\ \tilde{r}_s^{(l+1)}}{1 + \delta\coth(\delta)T_{\uparrow\downarrow}\left(\tilde{r}_s^{(l)} + \tilde{r}_s^{(l+1)}\right) + \delta^2 T_{\uparrow\downarrow}^2\tilde{r}_s^{(l)}\tilde{r}_s^{(l+1)}} \tag{13}$$

From these expression, one can extract the total spin-loss A_l at the interface l according to : $T_l + R_l + A_l = 1$ (an equivalent expression exists for the tilde equations).

2. Multiple interfaces: the scattering path approach and overall scattering matrix

The self-consistent treatment describing the multiple scattering process within the multilayer is performed in the so-called *scattering path formalism*. We then employ a "superscattering" approach to propagate this single interface equation to a whole multilayer. Following this approach , we derive a superscattering matrix $\mathbb{S}$ such that:

$$\mathbb{S}_{ij} = \tilde{S}_i \delta_{ij} + \mathbb{S}_{il} \mathbb{G}_{0,lj} \tilde{S}_j$$

or:

$$\mathbb{S}_{\mu\nu} = \left[\tilde{S}^{-1} \otimes \delta - \mathbb{G}_0\right]^{-1}_{\mu\nu}$$

with δ the $N \times N$ unity matrix (N is the number of interfaces) and $\mathbb{G}_0^{lj}$ the propagation matrices from the two neighboring interfaces l and j ($l = j \pm 1$) defining thus two different 2×2 matrices $\mathbb{G}_0^{l\ (l+1)}$ and $\mathbb{G}_0^{(l+1)\ l}$, the so-called propagator or Green's function of the out-of-equilibrium spin accumulation and currents between two neighboring interfaces (l) to the interface (l+1) (or vice versa).

The two different (complex) propagation matrix required for $n = l+1$ ($\mathbb{G}_0^{n,n+1}$) and $n = l-1$ ($\mathbb{G}_0^{n+1,n}$) write respectively:

$$\mathbb{G}_0^{n,n+1} = \begin{bmatrix} 0 & 0 \\ \exp\left(-\frac{t_{n+1}}{\tilde{\lambda}_{s,n+1}}\right) & 0 \end{bmatrix}; \mathbb{G}_0^{n+1,n} = \begin{bmatrix} 0 & \exp\left(-\frac{t_{n+1}}{\tilde{\lambda}_{s,n+1}}\right) \\ 0 & 0 \end{bmatrix} \tag{14}$$

(15)

We remind that the previous equations for $\mathbb{S}$ describing the multiple scattering approach and obeys the scheme of a perturbation potential $\hat{V}$ leading to the definition of the transition matrix $\hat{T}$ with:

$$\hat{T} = \hat{V} + \hat{V}\mathbb{G}_0\hat{T} \tag{16}$$

together with

$$\mathbb{G} = \mathbb{G}_0 + \mathbb{G}_0\hat{V}\mathbb{G} \tag{17}$$

We remind that $\tilde{S}_l$ are the single interface scattering matrix of the interface (l) entering as a diagonal block matrix in such 'supermatrix'. The supermatrix $\mathbb{S}_{\mu\nu}$ describes the scattering properties of the spin-current at the level of the interface μ we are searching for from an injection of an *effective spin current source* (SHE or Rashba) occurring at the interface ν.

C. Semi-classical modeling of SHE and REE

We choose to model Pt|Co||Al*, Pt|Co||Al|Pt and Pt|Co||$\tilde{Pt}$|Al systems as a stacking of four/five different layers Pt|Co|R|$\tilde{Al}$ characterized by their own effective propagation length and their own spin-resistance, and four different interfaces where $|| = |R|$ stands for the effective interfacial *confined orbital Rashba layer* to consider. $\tilde{Al}$ represents either Al|Pt or Pt|Al of respective effective spin-resistance $r_{Al} + r_s^{Pt}$ (r_{Al} is the Al layer resistance here) and $r_s^{Pt}\left(\frac{r_s^{Al} + r_s^{Pt}\tanh(t_{Pt})}{r_s^{Pt} + r_s^{Al}\tanh(t_{Pt})}\right) = \left(\frac{1}{G_{sf}}\right)$ which are clearly not identical in reversing the order of the Al|Pt bilayer.

The SHE layer(s) are representing by Pt (of spin resistance r_{Pt}^s), the Co ferromagnetic layer is represented by a complex relaxation length (complex spin resistance r_{Co}^{s*}) whereas the Al layer is the light metal characterized by a large spin-resistance r_s^{Al}.

Note that the Rashba interface is then represented by a virtual "interfacial" layer possibly having small transmission coefficients toward the neighbouring metallic layers (case of a confined interfacial state). In the case where such transmission is non zero, it stands for a small coupling existing between the interfacial evanescent Rashba states, which are evanescent wave functions, and bulk Bloch states. Since those two types of quantum electronic states are in principal orthogonal, this transmission coefficient remain in any case small compared to 1. This tiny transmission results in a pretty large spin accumulation inside this

virtual layer representing the Rashba-Edelstein effect, described more in details hereafter.

The overall SOT/OT in Co is the sum of three different terms: *(i)* the SOT emerging from the SHE of Pt, either from both side, and integrated over the ferromagnet thickness t_{Co} (Eqn. 6), *(ii)* the SOT due to the angular momentum accumulation in the virtual interface layer, and *(iii)* the SOT due to diffusion of this interfacial accumulation inside the 'bulk' Co, also integrated over t_{Co}. The damping like component is given by the real part of the SOT while the field-like torque is given by the imaginary part.

1. *Spin-Hall Currents*

The spin-Hall current generated by outward Pt layers can be generally described by a spin-current source $\Delta J_\sigma^\Sigma = \theta_{SHE} J_C$ incoming from the leftward (case of Fig. 2(b)) or from the rightward boundary. Our multiple scattering approach allows to satisfy the interfacial conditions described in the previous section. More generally, a SHE layer inside a multilayer may be modeled by sharing the spin-current source ΔJ_σ^Σ into two sub spin-current sources of weight $\frac{1}{2}$ impinging the respective left and right interfaces (case of Fig. 2(a)). That way, one can be easily be convinced that the interfacial conditions at both sides. As the spin-Hall effect in Pt admits Time-reversal symmetry properties (TRS), the resulting calculation is independent on the application of TRS (changing angular momentum flow and direction at the same time). It results that SHE applying to an infinitely thin layer is accompanied with zero angular momentum angular moment injection current.

2. *Rashba-Edelstein effect: introduction of a virtual interfacial layer*

We now discuss the modeling of Rashba contributions via the consideration of a virtual interfacial layer. The spin accumulation generated via the Rashba-Edelstein effect at a given interface 'i' can be modeled by considering an infinitely thin layer 'i' location of two opposite spin-up current sources $\Delta j_\sigma^{\Sigma_L}$ and $\Delta j_\sigma^{\Sigma_R}$ impinging the two interfaces (Fig. 2(c)). The separation into two opposite

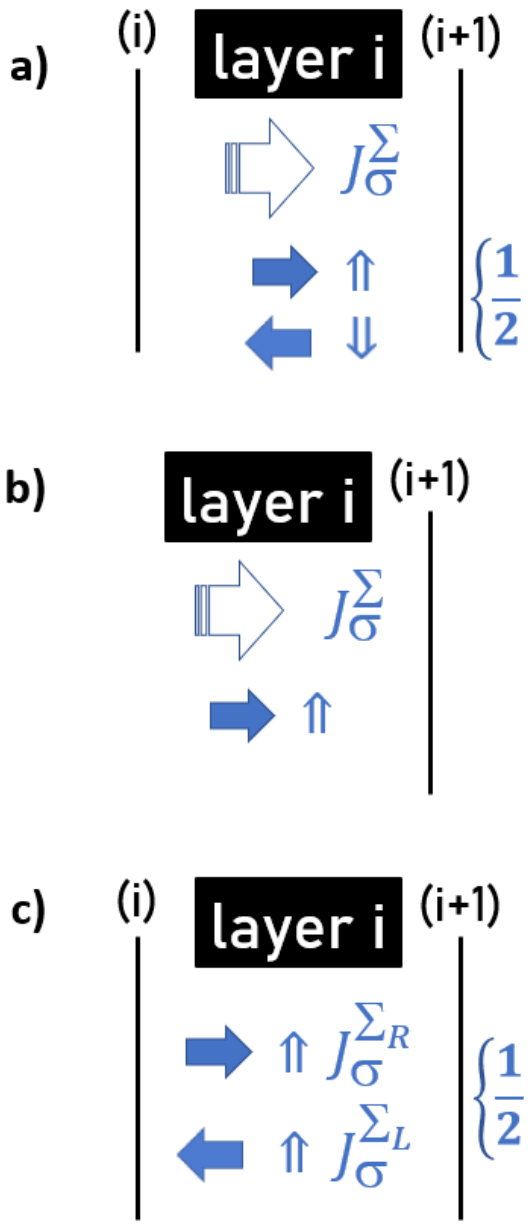

FIG. 2. Scheme of both SHE and Rashba-Edelstein process in a multiple scattering picture with the definition of the corresponding spin-current sources. (a) Case of SHE current within the layer 'i' described by a spin-current source J_σ^Σ. The spin-current can be decomposed into a spin-up propagating spin-current towards the right and a spin-down current towards the left (b) Case of SHE current injected from the outward left boundary. (c) Case of Rashba-Edelstein effect occurring at the interface layer 'i' which is composed of two opposite propagating currents of the same spin.

spin flow, as exploited in the scattering path formalism, generates a spin accumulation although the overall spin-current is zero in this case. The 2D orbital or spin accumulation $\check{\tilde{\mu}}$ then writes $\check{\tilde{\mu}} \simeq e\mathcal{N}_{DOS}^{2D}\left(\frac{r_L^* r_R^*}{r_L^*+r_R^*}\right)\Delta J_\sigma^\Sigma \simeq \left(e\theta_{REE}\mathcal{N}_{DOS}^{2D} r_L^* \sigma_{xx}\right)\mathbf{E} \simeq \left(e\theta_{REE}\lambda_{sf}\mathcal{N}_{DOS}^{2D}\right)\ \mathbf{E} = \left(e\lambda_{REE}\mathcal{N}_{DOS}^{2D}\right)\ \mathbf{E}$ (θ_{REE} and λ_{sf} are respectively the equivalent REE theta angle and effective spin-flip time whereas their product equals the REE length λ_{REE} scaling the orbital moment - charge conversion). It turns out that the Rashba response χ_{xy}^{REE} reads $\chi_{xy}^{REE} = \left(e\lambda_{REE}\mathcal{N}_{DOS}^{2D}\right)$. Considering $\theta_{REE} \simeq 0.1$ and $\lambda_{sf} \simeq 10$ nm, we find $\chi_{xy}^{REE} \simeq 10^{10}(\hbar)/(V.m)$ as expected.

In the limit of an infinitely thin interfacial layer (i), $\Delta\hat{J}_\sigma^{\Sigma_R}$ gives the same result than $\Delta\hat{J}_\sigma^{\Sigma_L}$ owing to the TRS property acting on an angular momentum accumulation.

3. Modeling results

In our model, the low transmission coefficients that we impose on that layer mechanically lead to simulating a large angular momentum accumulation because spins are not able to "escape". To exhibit that clearly, we simulated four cases:

1. A case where Al spin resistance (here dimensionless) is of 2, a value close to Co resistivity (2.5) and the two transmission coefficients are set to a small value: 0.1 (blue line on figure 3(c).
2. A case (orange line on figure 3(c) where the transmission toward Co is increased to 0.8.
3. A case (green line on figure 3(c) where the transmission coefficient toward Al is risen to 0.8 while the one toward Co is kept to 0.1.
4. In the last case, the transmission coefficient toward Al is again large (0.8) but the resistivity of Al is increased to 10.

Comparing the second case to the first, we see a reduction in the field-like torque despite a better transmission of spins from the virtual layer to Co. This

counter-intuitive result stems from the fact that increased transmission lowers the accumulation of spins more than it increases the angular momentum transfer. In the third case, the field like torque is the lowest because not only transmission of spins to Co is low but also electrons diffuse the best inside the Al layer where they exert no torque.

Finally, the fourth case recovers the same amplitude of field like torque as the first case due to the rise in Al resistivity. This is expected since a great resistivity difference between two consecutive layers prevents electronic diffusion equivalently to low transmission.

This model reproduces expected behavior of REE on SOT. The resulting torques are a trade off in the coupling of the Rashba states with the neighbouring metals: while better coupling with the ferromagnetic states improves transfer of angular momentum, it also decreases the lifetime of Rashba polarized electronic states and therefore the total amount of out of equilibrium momentum accumulation.

D. Rashba-Edelstein effect (REE) at Co|Al interfaces

The large increase in the experimental ratio ξ_{FL}/ξ_{DL} in Ta(5)|Pt(8)|Co(t_{Co})|Al|Pt(3) and Ta(5)|Pt(8)|Co(t_{Co})|Al* samples with ultrathin Co incompatible with a model comprising only Pt SHE and mostly real spin-mixing conductance at Pt|Co interface.

When the Rashba term is turned on through a non-zero source term in the virtual interfacial layer, we are able to precisely match the experimental data for each SOT component. This ultimately leads us to the conclusion that there exists a strong interfacial SOT generation at Co|Al interface through spin or orbital Rashba-Edelstein effect.

- The spin Hall effect (SHE) arising from the bottom Pt|Co layer is parameterized by a bare spin-angle angle of $\theta_{SHE} = 0.22 \pm 0.02$ and a spin-memory loss coefficient $\delta = 0.4$. Such SHE spin current is also subject to spin-backflow at this interface. The efficiency of the torques calculated for $t_{Co} = 0.9$ nm are respectively $\xi_{DL}^{SHE} = 0.045$ and $\xi_{FL}^{SHE} = 0.03$.

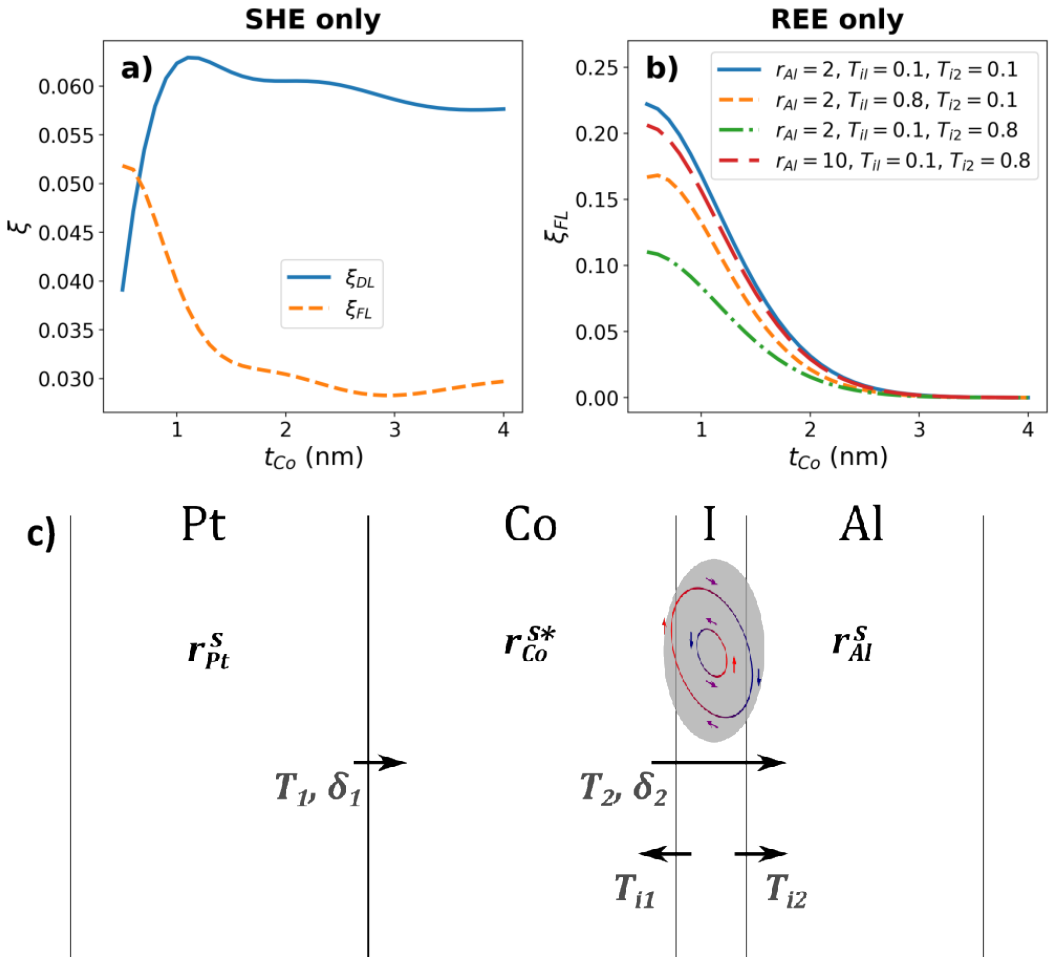

FIG. 3. (a) respective Field-like and Damping-like components of SOT due to SHE, no REE, dependence on Co layer thickness. (b) Field-like torque for different values of the parameters representing Al resistivity and the virtual Rashba layer transmission coefficients. SHE set to zero, dependence on Co layer thickness. (c) Scheme of the model for Pt|Co|Al multilayers with relevant coefficients. T_1 and T_2 represent the transmission coefficient between adjacent layers whereas T_{i1} and T_{i2} represent transmission from layers to interface Rashba states. δ_1 and δ_2 are spin-memory loss coefficients.

- The Ta(5)|Pt(8)|Co(0.9)|Al(1.4)|Pt(3) sample experiments OREE giving rise to *additional torque* components $\xi_{DL}^{OREE} = 0.03$ and $\xi_{FL}^{OREE} = 0.075$. The FLT from OREE represents 70% of this additional OREE torque (DLT represents 30%) showing the major role of REE to generate the FLT. This ratio is parameterized by the $T_{iL} \simeq 0.2$ transmission coefficient (coupling) from the Rashba virtual layer to bulk Co states as discussed by Rojas-Sanchez et al. [6]. The

OREE represents then 40% of the total DLT and 70% of the total FLT.

- The Ta(5) | Pt(8) | Co(0.9) | Al(3) | Pt(3) sample experiments OREE giving rise to additional torque components $\zeta_{DL}^{OREE} = 0.07$ and $\xi_{FL}^{OREE} = 0.21$, still compared to SHE. The Field-like torque by OREE then represents 75% of this additional OREE torque (DLT is only 25%). This ratio is parameterized by a coupling $T_{iL} \simeq 0.1$ (transmission coefficient) from the Rashba to bulk Co states.

- Those calculations reproduce then well the amplitude of the experimental torques reported here. The final conclusion is that, Ta(5) | Pt(8) | Co(0.9) | Al(1.4) | Pt(3) and Ta(5) | Pt(8) | Co(0.9) | Al(3) | Pt(3) samples, the total DLT efficiency increases from $\xi_{DL} = 0.075$ to $\xi_{DL} = 0.12$ whereas for the FLT , the increase goes from $\xi_{FL} = 0.11$ to $\xi_{FL} = 0.23$.

The reduced critical switching current observed in the Co | Al sample can thus be assigned to the ability of the OREE to enhance the damping-like component of the SOT. While OREE is typically associated with a dominant FL torque, our switching experiments demonstrate its effectiveness as a powerful tool for probing the DLtorque and, more broadly, for torque metrology. Table III summarizes the measured values and relative contributions of both torque efficiencies, ξ_{FL} and ξ_{DL} efficiencies for the two samples.

	ξ_{FL}			ξ_{DL}		
Ta(5) | Pt(8) | Co(0.9) | Al(1.4) | Pt(3)	SHE	OREE	total	SHE	OREE	total
	0.025	0.075	0.10	0.0375	0.03	0.0675
	25 %	75 %	100 %	56 %	44 %	100 %
Ta(5) | Pt(8) | Co(0.9) | Al(3) | Pt(3)	SHE	OREE	total	SHE	OREE	total
	0.03	0.21	0.24	0.045	0.07	0.115
	13 %	87 %	100 %	39 %	61 %	100 %

TABLE III. Values and relative contributions of OREE and Pt SHE in both torque ξ_{FL} and ξ_{DL} efficiencies for the two samples. For instance, in Ta(5) | Pt(8) | Co(0.9) | Al(3) | Pt(3), SHE induces 0.03 field like efficiency and OREE 0.21. OREE thus induces 87 % of the field like torque.

[1] C. Petitjean, D. Luc, and X. Waintal, Unified drift-diffusion theory for transverse spin currents in spin valves, domain walls, and other textured magnets, Phys. Rev. Lett. **109**, 117204 (2012).

[2] R. V. Shchelushkin and A. Brataas, Spin hall effect, hall effect, and spin precession in diffusive normal metals, Phys. Rev. B **72**, 073110 (2005).

[3] C. O. Pauyac, M. Chshiev, A. Manchon, and S. A. Nikolaev, Spin hall and spin swapping torques in diffusive ferromagnets, Phys. Rev. Lett. **120**, 176802 (2018).

[4] T. Jungwirth, J. Wunderlich, V. Novák, K. Olejník, B. L. Gallagher, R. P. Campion, K. W. Edmonds, A. W. Rushforth, A. J. Ferguson, and P. Němec, Spin-dependent phenomena and device concepts explored in (ga,mn)as, Rev. Mod. Phys. **86**, 855 (2014).

[5] S. Krishnia, B. Bony, E. Rongione, L. M. Vicente-Arche, T. Denneulin, A. Pezo, Y. Lu, R. Dunin-Borkowski, S. Collin, A. Fert, et al., Quantifying the large contribution from orbital rashba–edelstein effect to the effective damping-like torque on magnetization, APL Materials **12** (2024).

[6] J. R. Sánchez, L. Vila, G. Desfonds, S. Gambarelli, J. Attané, J. De Teresa, C. Magén, and A. Fert, Spin-to-charge conversion using rashba coupling at the interface between non-magnetic materials, Nature communications **4**, 2944 (2013).